Zhenzhen Wang, Yoshihiro Deguchi, Renwei Liu, Akihiro Ikutomo, Zhenzhen Zhang, Daotong Chong, Junjie Yan, Jiping Liu, Fang-Jung Shiou, Emission Characteristics of Laser-Induced Plasma Using Collinear Long and Short Dual-Pulse Laser-Induced Breakdown Spectroscopy (LIBS) , Applied Spectroscopy (Volume: 71 issue: 9) pp. 2187-2198 . DOI: 10.1177/0003702817693239.

Emission characteristics of laser-induced plasma using collinear long and short dual-pulse LIBS

Zhenzhen Wang[1,2], Yoshihiro Deguchi[2,*], Renwei Liu[2, 3], Akihiro Ikutomo[2], Zhenzhen Zhang[3], Daotong Chong[1], Junjie Yan[1], Jiping Liu[3], Fang-Jung Shiou[4]

[1]State Key Laboratory of Multiphase Flow in Power Engineering, Xi'an Jiaotong University, Xi'an 710049, China

[2]Graduate School of Advanced Technology and Science, Tokushima University, Tokushima 770-8501, Japan

[3]Moe Key Laboratory of Thermo-Fluid Science and Engineering, Xi'an Jiaotong University, Xi'an 710049, China

[4]Department of Mechanical Engineering, National Taiwan University of Science and Technology, Taipei 10607, Taiwan

Corresponding author: Yoshihiro Deguchi

Graduate School of Advanced Technology and Science, Tokushima University

TEL: (+81)-88-656-7375

FAX: (+81)-88-656-9082

Email address:ydeguchi@tokushima-u.ac.jp

Postal address: 2-1, Minamijyosanjima, Tokushima 770-8506 Japan

Abstract

The collinear long and short dual-pulse LIBS (DP-LIBS) was employed to clarify the emission characteristics from laser-induced plasma. The plasma was sustained and became stable by the long pulse-width laser with the pulse width of 60 μs under FR (free running) condition as an external energy source. Comparing the measurement results of stainless steel in air using SP-LIBS and DP-LIBS, the emission intensity was enhanced using DP-LIBS markedly. The temperature of plasma induced by DP-LIBS was maintained at higher temperature under different gate delay time and short pulse-width laser power conditions compared with these measured using SP-LIBS of short pulse width. Moreover, the variation rates of plasma temperature measured using DP-LIBS were also lower. The superior detection ability was verified by the measurement of aluminum sample in water. The spectra were clearly detected using DP-LIBS, whereas it cannot be identified using SP-LIBS of short pulse width and long pulse width. The effects of gate delay time and short pulse-width laser power were also discussed. These results demonstrate the feasibility and enhanced detection ability of the proposed collinear long and short DP-LIBS method.

Keywords: Long pulse, DP-LIBS, Enhancement, Plasma temperature stabilization, Underwater measurement

Introduction

Laser-induced breakdown spectroscopy (LIBS) technique as a useful elemental composition determination method has been applied in various fields, such as space exploration, industrial processes, environment protection, food safety, etc. [1-6] due to its advantages of fast response, high sensitivity, non-contact and multi-elemental detection. The researches of LIBS fundamentals and applications have been extensively studied to improve LIBS technique. Most fundamental researches focus on the signal enhancement to improve the accuracy and detection ability of LIBS measurement, as well as understanding of the basic plasma physics. Various papers reported the signal enhancement by optimizing the experimental conditions to improve LIBS detection ability, such as pulse width, laser wavelength, laser power, gate delay time, lens-to-sample distances, atmospheric condition, etc.[7-11] Some improvement approaches of LIBS technique have also been developed, such as dual-pulse LIBS (DP-LIBS),[12-15] resonance-enhanced LIBS (RE-LIBS),[16,17] laser ablation fast pulse discharge plasma spectroscopy (LA-FPDPS),[18,19] microwave-assisted LIBS (MA-LIBS),[20] LIBS laser-induced fluorescence (LIBS-LIF)[21] and other combination methods.

DP-LIBS is an important way to enhance the emission intensities to improve LIBS analytical capability. The combinations of laser pulses with different pulse width, laser wavelength and laser power have been studied. Four geometrical configurations have been employed to realize DP-LIBS technique, such as collinear, crossed beam, orthogonal pre-ablation and orthogonal re-heating configurations.[22,23] MA-LIBS has

also been successfully demonstrated to enhance the emission intensity of plasma by increasing the lifetime of plasma to a few hundred microseconds.[24-26] In LIBS process, the atomic emission signals arise in the plasma cooling process. These techniques are conceptually similar as they employ an external energy source to sustain the plasma and to enhance the emission intensity. In MA-LIBS, the additional microwave device should be installed around the measurement target to cause the system complex, which may suffer some limitations in real applications. Usually, the second laser employed in DP-LIBS is Q-switched Nd:YAG laser. The second laser is not only to sustain the plasma but also to induce the plasma to some extent. The plasma generation processes become confused for analyses.

Nd:YAG-CO_2 DP-LIBS using a second and long pulse of 10.6 μm CO_2 laser pulse was applied to enhance the emission signal with the crossed beam configuration.[27-29] However, CO_2 laser is not suitable for the long distance measurement coupling with the optical fiber. The benefits of long pulse LIBS for underwater spectroscopy were reported to demonstrate an improvement in the quality of the signal observed by increasing the duration of the pulse used for ablation to 150 ns at hydrostatic pressures between 0.1 MPa and 30 MPa.[30,31] The timing of the bubble formation was examined by irradiating the target with two different pulse widths, 150 ns long pulse as the ablation laser and 20 ns short pulse under normal operating conditions with the orthogonal pre-ablation configuration.[32] There are several geometrical configurations for DP-LIBS as stated above. However, the collinear configuration is much more feasible in some real applications.

In this study, a new collinear long and short DP-LIBS method was proposed to improve the detection ability and measurement accuracy by the control of the plasma cooling process using the long pulse-width laser radiation. In this method, the laser-induced plasma was generated by the short pulse-width laser and the external energy was supplied by the long pulse-width laser with the pulse width of 60 μs under FR (free running) condition, which means the Q value of optical resonant cavity does not change during laser pulse formation, to sustain the plasma to improve the detection ability and feasibility in the real applications due to its collinear configuration. Fig.1 shows the notional comparison of laser-induced plasma processes of single-pulse LIBS (SP-LIBS), conventional DP-LIBS and long and short DP-LIBS. The plasma temperature and lifetime can be increased using DP-LIBS compared with SP-LIBS.[33,34] The plasma temperature is usually not uniform according to the spatial and temporal distribution. When using the conventional DP-LIBS, as shown in Fig.1(b), the plasma temperature can be enhanced. However, the temperature distribution is also not uniform and fluctuates. In the case of long and short DP-LIBS, the plasma temperature can be maintained at certain higher level along the long pulse-width laser path without obvious undesirable effect, even if the short pulse-width laser power becomes lower, as illustrated in Fig.1(c) and Fig.1(d). The plasma generated by the short pulse-width laser is stabilized and maintained at high temperature during the plasma cooling process by long pulse-width laser radiation. It is significant for laser-induced plasma processes. There are also other expected features of this method as described below.

1) There are the cleaning and pre-treatment effects of target surface by long pulse-width laser radiation in condition that the short pulse-width laser, which induces the plasma, is applied in the middle of the long pulse-width laser radiation.

2) Optical fiber delivery is easy for the long pulse-width laser radiation because peak laser intensity is low.

3) The self-absorption effect supposed to be reduced by restricting the hot plasma region by the long pulse-width laser radiation.

In this study, the solid samples, such as stainless steel in air and aluminum(Al) sample in water, were analyzed using this proposed method which is the first LIBS application to actively control and stabilize the LIBS plasma temperature temporally and spatially using long and short DP-LIBS. The enhancement mechanism and the experimental parameter effects were discussed to reveal the merits of this new proposed method.

Theory

The processes involved in LIBS are complex and the laser-induced plasma is not uniform. Plasma creation and evolution processes were analyzed and clarified including multi-photon ionization and electron impact ionization processes. Once ions are produced by the LIBS process, laser energy is absorbed intensively and plasma grows rapidly by electrons and the electron impact ionization process, that is, inverse bremsstrahlung absorption. After the termination of the laser pulse, the plasma continues expanding. Simultaneously, the three-body recombination proceeds and the temperature decreases gradually compared with the plasma generation process. LIBS

emission signals appears from this temporally and spatially non-uniform plasma. It is often the case that the electrons, ions or neutrals in plasma are not in local thermodynamic equilibrium (LTE) condition.[35,36] These effects was also analyzed by the theoretical model including multi-photon ionization and electron impact ionization processes.[37] On the other hand, most of the LIBS methods assume the spatially uniform plasma and the LTE condition to calculate the quantitative elemental analyses. This induces a decrease in the precision of LIBS quantitative analyses.

When low energy laser radiation is applied to the area of this cooling plasma, inverse bremsstrahlung absorption by this low energy laser radiation and the recombination can become equilibrium. Accordingly temporally and spatially uniform plasma can be attained in this region. This theoretical model is briefly described below and the details are shown elsewhere.[37] The laser light propagation is modeled using Maxwell equations as follows,

$$\nabla \times \mathbf{H} = \varepsilon \frac{\partial \mathbf{E}}{\partial t} + \mathbf{J} \qquad (1)$$

$$\nabla \times \mathbf{E} = -\mu \frac{\partial \mathbf{H}}{\partial t} \qquad (2)$$

In above equations, **H** and **E** are magnetic and electric fields respectively, ε and μ are permittivity and magnetic permeability, **J** is the current density because of movements of charged particles in plasma. The evolution processes of gas phase plasma (neutral, ion and electron) were modeled using Boltzmann equations. [37]

$$\frac{\partial f_{\mathrm{e}}}{\partial t} + \mathbf{v}_{\mathrm{e}} \cdot \nabla f_{\mathrm{e}} + \mathbf{a}_{\mathrm{e}} \cdot \nabla_{\mathbf{v}_{\mathrm{e}}} f_{\mathrm{e}} = -\frac{f_{\mathrm{e}} - f_{\mathrm{en}}^{\mathrm{eq}}}{\lambda_{\mathrm{en}}} + R_{\mathrm{e}} f_{\mathrm{e}}^{\mathrm{eq}} \qquad (3)$$

$$\frac{\partial f_{\mathrm{i}}}{\partial t} + \mathbf{v}_{\mathrm{i}} \cdot \nabla f_{\mathrm{i}} + \mathbf{a}_{\mathrm{i}} \cdot \nabla_{\mathbf{v}_{\mathrm{i}}} f_{\mathrm{i}} = -\frac{f_{\mathrm{i}} - f_{\mathrm{in}}^{\mathrm{eq}}}{\lambda_{\mathrm{in}}} + R_{\mathrm{i}} f_{\mathrm{i}}^{\mathrm{eq}} \qquad (4)$$

$$\frac{\partial f_{\mathrm{n}}}{\partial t} + \mathbf{v}_{\mathrm{n}} \cdot \nabla f_{\mathrm{n}} = -\frac{f_{\mathrm{n}} - f_{\mathrm{nn}}^{\mathrm{eq}}}{\lambda_{\mathrm{nn}}} + R_{\mathrm{n}} f_{\mathrm{n}}^{\mathrm{eq}} \qquad (5)$$

In equations (3) – (5), the subscript s (e, i or n) denotes the type of particles and takes e, i or n for electrons, ions or neutrals respectively. f_s is the distribution function, and f_s^{eq} is its value when the particle is in the equilibrium state. $\mathbf{v}_s$ is the microscopic velocity, $\mathbf{a}_s$ is acceleration of charged particles because of Lorentz force. λ_{en}, λ_{in} and λ_{nn} are relaxation times for electron-neutral, ion-neutral and neutral-neutral collisions. f_{en}^{eq}, f_{in}^{eq} and f_{nn}^{eq} are the equilibrium distribution functions in these collisions respectively. R_s is the number density change rate because of inelastic collisions, and it contains three parts: R_{sm} by multi-photon ionization, R_{si} by electron impact ionization and R_{sr} by three-body recombination.

f_e and f_i in equations (3) – (4) are reduced rapidly after the termination of the laser pulse because the source items of electrons and ions, i.e. R_{sm} and R_{si} (s: e or i) become zero. When the low energy laser radiation (long pulse-width laser) is applied to this cooling plasma, f_e and f_i become quasi-equilibrium depending on the laser fluence and plasma temperature in this region is stabilized temporally and spatially to make a uniform plasma. It also helps to attain the LTE condition by the maintaining quasi-equilibrium plasma condition temporally and spatially. Because LTE requires each local change slowly enough to practically sustain its local Maxwell–Boltzmann distribution.

Experiment

Fig.2(a) and Fig.2(b) illustrates the experimental setup of DP-LIBS consisting of two lasers, digital delay generator, fiber, spectrometer, ICCD (Intensified Charge Coupled Device) camera and auxiliary equipment. The nanosecond laser 1 (LOTIS TII, LS-2134UTF, 5-8 ns, 10 Hz, beam diameter: 6 mm) was operated at 532 nm with laser power of dozens of milli-joule and the pulse width of 5-8 ns under normal operating conditions. The nanosecond laser 2 (LOTIS TII, LS-2137U, 6-8 ns, 10 Hz, beam diameter: 8 mm) was operated at 1064 nm with the pulse width of 60 μs under FR (free running) condition. Its laser power was set to 400 mJ/pulse and 500 mJ/pulse for different experiment to stabilize and maintain the plasma. The inter-pulse delay time between these two lasers was adjusted by the digital delay generator (Stanford Research Systems, Model DG645) and verified by the oscilloscope (Tektronix, MDO3014). Fig.2(c) and Fig.2(d) shows the schematic diagram of measured shapes of two pulses and different delay time. In order to determine the inter-pulse delay time, the shape of short and long pulse-width laser radiations were monitored at the combining point of long and short pulse-width lasers. The gate delay time of ICCD was triggered by the short pulse-width laser under all experimental conditions. SP-LIBS was performed by setting either of the long or short pulse-width laser power to be zero. These two laser beams were focused on the samples under collinear configuration using different focal lenses. Each focal lens with focal length of 300 mm was employed for 1064 nm and 532 nm laser beams and then the focused laser beams employed collinear configuration for stainless steel measurement in air, as shown in Fig.2(a). The optical setup for Al sample measurement in water is shown in Fig.2(b). 1064 nm and 532 nm laser beams

employed collinear configuration and then were focused on the target using the focal lens with focal length of 80 mm due to the necessity of higher energy density to induce plasma for underwater measurement. Emission signals from the plasma of the measurement samples were focused on the fiber using a focal lens with focal length of 100 mm and detected by the combination of a spectrometer (SOL, NP-250-2M), an ICCD camera (Andor, iStar DH334T-18U-03), and auxiliary equipment. The grating of spectrometer employed was 300 l/nm with the resolution of 0.15 nm/pixel and the spectra range of 235nm-385nm.

Measurement results of stainless steel in air

Stainless steel in air was measured using SP-LIBS of short pulse width, SP-LIBS of long pulse width and DP-LIBS under different conditions. Measured spectra in different measurement conditions were shown in Fig.3. The detection features were discussed in various inter-pulse delay time, gate delay time and short pulse-width laser power conditions. Fig.3(a) shows the comparison of measured spectra using DP-LIBS and SP-LIBS. The signals were normalized with respect to maximum signal using DP-LIBS. As is well known, there are numerous Fe emission lines. According to the measurement results, several representative wavelength ranges of Fe emission were determined. The emission intensity was summed as these wavelength ranges. In each wavelength range, Fe specific emission lines and their corresponding parameters were checked using the database and listed as data range in Table 1.[38] In every Fe wavelength range, there are also many Fe emission lines including atomic and ionic emission lines.

The data range of upper level energy and Einstein A coefficient were listed in Table 1 for the conspicuous and representative Fe emission line groups in each Fe wavelength range. The distinct spectra were observed when using SP-LIBS of short pulse width and DP-LIBS, whereas the spectra cannot be identified from SP-LIBS measurement of long pulse width. It is recognized that the long pulse-width laser was unable to make plasma to generate LIBS signals. It can also be seen that the emission intensity was enhanced obviously when using DP-LIBS. In LIBS process, the core of plasma is first produced by the absorption of the incident laser energy. Once the initial free electrons are produced, laser photons are also absorbed through inverse bremsstrahlung absorption to induce rapid expansion of plasma. When introducing the external energy from the long pulse-width laser during the plasma cooling process, the inverse bremsstrahlung absorption can appear[37] in this process to maintain the plasma at higher and constant temperature. It also extends the plasma lifetime. Therefore the emission intensity from plasma can be improved. In order to clarify this phenomenon, the detection ability and features between SP-LIBS of short pulse width and DP-LIBS were evaluated under various experimental conditions, such as inter-pulse delay time, gate delay time and short pulse-width laser power.

The measured spectra using SP-LIBS of short pulse width and DP-LIBS were compared and discussed in detail under a specific condition. Fig.3(b) shows the measured spectra in gate delay time of 4000 ns using SP-LIBS of short pulse width and DP-LIBS. The signals were normalized with respect to signal of Fe-5 using SP-LIBS and DP-LIBS, respectively. When comparing the measured spectra in the same gate delay time,

the emission lines of Fe-1, Fe-2 and Fe-4 were enhanced more compared with other signals using DP-LIBS. Fe-1, Fe-2 and Fe-4 emission signals are attributed to those from higher upper level energy compared with other emissions. The absolute emission intensity of Fe lines was enhanced obviously when using DP-LIBS as shown in Fig.3(a). Fig.3(c) shows the measured spectra using SP-LIBS of short pulse width and DP-LIBS at short pulse-width laser power of 23 mJ/pulse. The signals were normalized with respect to signal of Fe-5 using SP-LIBS and DP-LIBS, respectively. When comparing the measured spectra at the same short pulse-width laser power, the emission lines with higher upper level energy, such as Fe-1, Fe-2 and Fe-4, displayed the enhanced emission signals using DP-LIBS. The quantitative analyses of various parameters were discussed as follows.

Effect of inter-pulse delay time

The inter-pulse delay time between two lasers is an important parameter for DP-LIBS. The stainless steel in air was measured using DP-LIBS in different inter-pulse delay time. Fig.4(a) shows the inter-pulse delay time dependence of several Fe emission signals. The emission intensity increased first and then decreased when increasing the inter-pulse delay time, which shows the similar profile to the long pulse-width laser shape. This result agrees to the long pulse-width laser function. It is demonstrated that the long pulse-width laser does not make plasma to generate LIBS signals and just sustains the plasma induced by the short pulse-width laser in high temperature condition. The time scale of plasma generation and growth processes is usually tens of nanoseconds depending on the conditions.[39] The emission intensity ratio from the same

atom with different upper level energy can be employed as the temperature indicator to discuss the detection features. The emission intensity ratio of Fe-4 to Fe-5 (I_{Fe-4}/I_{Fe-5}) was used to evaluate the inter-pulse delay time effect, as shown in Fig.4(b). When increasing the inter-pulse delay time, I_{Fe-4}/I_{Fe-5} increased slightly. It is demonstrated that the plasma temperature can be maintained at certain level. The atomic emission signals arise in the plasma cooling process, which is very essential for signal detection. Therefore, the inter-pulse delay time between two lasers affects the conservation of plasma temperature during the plasma cooling process to sustain the atomic emission signals. The optimal inter-pulse delay time to sustain the plasma was determined according to these measurement results. Consequently, the effects of gate delay time and short pulse-width laser power were evaluated to compare the detection ability of SP-LIBS of short pulse width and DP-LIBS in inter-pulse delay time of 25 μs.

Gate delay time effect of SP-LIBS and DP-LIBS

The stainless steel in air was measured using SP-LIBS of short pulse width and DP-LIBS in different gate delay time. The enhancement ratio of signal intensity using DP-LIBS compared with that using SP-LIBS of short pulse width was shown in Fig.4(c). When comparing the enhancement ratios of Fe-3, Fe-4, Fe-5 and Fe-6 in different gate delay time, Fe-4 was enhanced notably because of its higher upper level energy. The emission intensity from upper levels with higher energy is more sensitive to plasma temperature compared with that with lower energy. I_{Fe-4}/I_{Fe-5} was employed to compare the measurement results using SP-LIBS of short pulse width and DP-LIBS, as shown in Fig.4(d). I_{Fe-4}/I_{Fe-5} measured by DP-LIBS were higher than these measured by SP-

LIBS of short pulse width, which means the plasma temperature was maintained at higher temperature using DP-LIBS. When increasing the gate delay time, the intensity ratios decreased. One reason for this is the different upper level energy of each emission line. The emission intensity of Fe-4 presented a relatively quick decline as increasing the gate delay time due to emission lines with higher upper level energies compared with the emission lines of Fe-5. Additionally, the decrease rate of DP-LIBS was lower compared with that using SP-LIBS of short pulse width. When employing the long pulse-width laser to sustain the plasma, the plasma decay was deferred to extend the plasma lifetime. This effect was valid more than 6000 ns under these experimental conditions.

Short pulse-width laser power effect of SP-LIBS and DP-LIBS

The plasma was induced by the short pulse-width laser when using long and short DP-LIBS. The short pulse-width laser power effect on emission signals was discussed in gate delay time of 2000 ns. The enhancement ratio of signal intensity using DP-LIBS compared with that using SP-LIBS of short pulse width was shown in Fig.4(e). The emission signals were improved obviously using DP-LIBS, especially at lower short pulse-width laser power. The signal to noise ratio (SNR) was also compared at different short-pulse width laser power between DP-LIBS and SP-LIBS. The signal intensity (S) was defined as the peak of each wavelength range. The noise (N) was the standard deviation of emission intensity around 240nm-242nm. The reason for the wavelength range of noise was that the emission signals can be observed between 245nm-385nm. The enhancement ratio of SNR shown in Fig.4(f) displayed the concordant results with

the enhancement ratio of signal intensity. In the same condition, the enhancement ratio of SNR was slightly lower than that of the enhancement ratio of signal intensity. When employing DP-LIBS, the noise increased slightly, whereas, the emission signals were improved obviously. The plasma temperature can be maintained stable at higher temperature level, which mainly contributed to the signal emission intensity.

I_{Fe-4}/I_{Fe-5} using DP-LIBS was higher than that using SP-LIBS of short pulse width, as shown in Fig.4(g). It is also demonstrated that the higher plasma temperature using DP-LIBS was attained, which shows the consistent results with the gate delay time effect. I_{Fe-4}/I_{Fe-5} increased with increase in the short pulse-width laser power. Because Fe-4 with its higher upper level energy showed a relatively quick increase as increasing the short pulse-width laser power compared with the emission intensity of Fe-5. Comparing I_{Fe-4}/I_{Fe-5} between SP-LIBS and DP-LIBS, I_{Fe-4}/I_{Fe-5} by DP-LIBS was almost constant. The plasma was sustained by the long pulse-width laser radiation as an external energy without obvious undesirable effects. This means that long and short DP-LIBS can control the plasma at cooling process to be insensitive to the initial plasma generation process and stabilize the plasma emission condition of LIBS measurement period. This feature is one of the merits of long and short DP-LIBS.

It is worth noting that, comparing the measurement results in Fig.4(b), Fig.4(d) and Fig.4(g), I_{Fe-4}/I_{Fe-5} presents the averaged value of 0.44 using SP-LIBS and 0.61 using DP-LIBS under various conditions, as listed in Table 2. It is demonstrated that the temperature was maintained at certain higher temperature level even if under various conditions using DP-LIBS. According to the results shown in Table 2, the plasma was

sustained by the long pulse and became stable. The signal emission intensity was enhanced obviously using DP-LIBS compared with that using SP-LIBS. For example, the enhancement ratios of Fe-4 and Fe-5 were 4.8-37.4 and 3.0-23.0 under different gate delay time and short pulse-width laser power conditions.

Measurement results of Al sample in water

LIBS detection ability for stainless steel measurement in air was improved using the proposed DP-LIBS method. The lifetime of plasma was extended when employing the long pulse-width laser to sustain the plasma. The difficulty for underwater measurement is the short lifetime of plasma. Therefore, the Al sample in water was also measured using this method under various experimental conditions to verify its superior detection ability.

Comparison of Al sample in air and water

An Al sample in air was measured first using SP-LIBS of short pulse width in different gate delay time to identify the detectable emission lines from Al sample, as shown in Fig.5(a) in gate delay time of 200 ns. The emission lines from Al samples and the self-absorption effect of Al lines have been investigated by experimental analyses of LIBS spectra in some papers,[40,41] which demonstrate the corresponding measured spectral lines in this study. The spectral parameters of different observed lines of Al sample are listed in Table 3.[38,42-46] The emission intensity ratio of Mg-1 to Mg-2 (I_{Mg-1}/I_{Mg-2}) was employed to evaluate its emission features. Fig.5(b) shows the gate delay time dependence of I_{Mg-1}/I_{Mg-2}, which decreased rapidly in shorter gate delay time.

Theoretical dependence of I_{Mg-1}/I_{Mg-2} on plasma temperature is shown in Fig.5(c).[38] I_{Mg-1}/I_{Mg-2} was normalized at 2000 K to compare the tendency of I_{Mg-1}/I_{Mg-2} dependence on plasma temperature. I_{Mg-1}/I_{Mg-2} increased rapidly at higher temperature, which is consistent with the experimental result.

Fig.6(a) shows the comparison of Al sample measurement results in water using SP-LIBS and DP-LIBS. The signals were normalized with respect to maximum signal using DP-LIBS. The spectra were recognized using neither SP-LIBS of short pulse width nor SP-LIBS of long pulse width. However, the distinguishable emission lines were detected using DP-LIBS. It demonstrates the feasibility for underwater measurement. According to the measurement results of DP-LIBS in different inter-pulse delay time, the optimal inter-pulse delay time was set in 25 μs.

Al sample measurement in water using DP-LIBS

An Al sample in water was measured in different gate delay time using DP-LIBS. The lifetime of plasma under water is shorter than that in air. The gate delay time employed here was set to be less than 100 ns. Fig.6(b) shows the gate delay time dependence of I_{Mg-1}/I_{Mg-2} using DP-LIBS. When increasing the gate delay time, I_{Mg-1}/I_{Mg-2} decreased. The results can be explained by the fact that the ionic emission line of Mg-1 decreased faster compared with the atomic emission line of Mg-2 when increasing the gate delay time, which means the decrease of plasma temperature. The Al sample was also measured under different long pulse-width laser power. Distinguishable Al signals by different long pulse-width laser powers of 420, 500, and 620 mJ/pulse were detected

until the gate delay times of 50, 80, and 120 ns, respectively. It is considered that the continuance of plasma in water depends on the long pulse-width laser energy density.

The effect of short pulse-width laser power on emission signal using DP-LIBS was also investigated in gate delay time of 40 ns. The short pulse-width laser power dependence of I_{Mg-1}/I_{Mg-2} was shown in Fig.6(c). When increasing the short pulse-width laser power, I_{Mg-1}/I_{Mg-2} increased slightly. Because the plasma can be sustained by the long pulse-width laser as the external energy using DP-LIBS according to the above results, the emission intensity was not sensitive to the short pulse-width laser energy, which shows the stabilization of the plasma condition using DP-LIBS. The measurement results demonstrate the feasibility of DP-LIBS for LIBS measurements in water.

Conclusions

A new collinear long and short DP-LIBS method was proposed in this study. The external energy source was supplied by the long pulse-width laser with the pulse width of 60 μs under FR (free running) condition to sustain the plasma. The plasma became stable and it was maintained at higher temperature to improve LIBS detection ability and feasibility for applications. The stainless steel in air and Al sample in water were measured using the proposed DP-LIBS method to evaluate its detection features.

The emission intensity of stainless steel measurement in air was enhanced using DP-LIBS compared with that using SP-LIBS of short pulse width. However, the long pulse-width laser was unable to make plasma to generate LIBS signals using SP-LIBS of long pulse width. The gate delay time effect and short pulse-width laser power effect were

discussed to compare the detection features of SP-LIBS of short pulse width and DP-LIBS. Because the plasma was sustained by the long pulse-width laser as an external energy source, the temperature of plasma induced by DP-LIBS was maintained at higher temperature and became stable under various conditions, such as inter-pulse delay time, gate delay time and short pulse-width laser power. In the case of Al sample measurement in water, the spectra can be distinguished using DP-LIBS, whereas, the spectra cannot be identified using SP-LIBS of short pulse width and long pulse width. The gate delay time effect and short pulse-width laser power effect were also discussed. The measurement results verify the applicability of DP-LIBS for LIBS measurements in water. These results presented here demonstrate the feasibility and detection enhancement of the proposed collinear long and short DP-LIBS.

Acknowledgements

This work was supported by National Natural Science Foundation of China (No. 51506171, 51436006), the National Key Basic Research Development Plan (No. 2015CB251504), Postdoctoral Science Foundation of China (No. 2015M582655) and the joint research fund between Tokushima University and National Taiwan University of Science and Technology.

References

[1] J.B. Sirven, B. Salle, P. Mauchien, J.L. Lacour, S. Maurice, G. Manhes. “Feasibility Study of Rock Identification at the Surface of Mars by Remote Laser-Induced Breakdown Spectroscopy and Three Chemometric Methods”. J. Anal. At. Spectrom. 2007. 22(12): 1471-1480.

[2] Z.Z. Wang, Y. Deguchi, M. Kuwahara, T. Taira, X.B. Zhang, J.J. Yan, J.P. Liu, H. Watanabe, R. Kurose. “Quantitative Elemental Detection of Size-Segregated Particles using Laser-Induced Breakdown Spectroscopy”. Spectrochim. Acta Part B. 2013. 87: 130-138.

[3] S. Kashiwakura, K. Wagatsuma. “Rapid Sorting of Stainless Steels by Open-Air Laser-Induced Breakdown Spectroscopy with Detecting Chromium, Nickel, and Molybdenum”. ISIJ Int. 2015. 55(11): 2391-2396.

[4] R. Noll. Laser-Induced Breakdown Spectroscopy: Fundamentals and Applications. Germany: Springer, 2012.

[5] M.Y. Yao, L. Huang, J.H. Zheng, S.Q. Fan, M.H. Liu. “Assessment of Feasibility in Determining of Cr in Gannan Navel Orange Treated in Controlled Conditions by Laser Induced Breakdown Spectroscopy”. Opt. Laser Technol. 2013. 52: 70-74.

[6] D.W. Hahn, N. Omenetto. “Laser-Induced Breakdown Spectroscopy (LIBS), Part II: Review of Instrumental and Methodological Approaches to Material Analysis and Applications to Different Fields”. Appl. Spectrosc. 2012. 66(4): 347-419.

[7] Z.Z. Wang, Y. Deguchi, J.J. Yan, J.P. Liu. “Comparison of the Detection Characteristics of Trace Species using Laser-Induced Breakdown Spectroscopy

and Laser Breakdown Time-of-Flight Mass Spectrometry". Sensors. 2015. 15: 5982-6008.

[8] Z.Z. Wang, Y. Deguchi, M. Kuwahara, J.J. Yan, J.P. Liu. "Enhancement of Laser-Induced Breakdown Spectroscopy (LIBS) Detection Limit using a Low-Pressure and Short-Pulse Laser-Induced Plasma Process". Appl. Spectrosc. 2013. 67(11): 1242-1251.

[9] Y. Zhang, Y.H. Jia, J.W. Chen, X.J. Shen, L. Zhao, C. Yang, Y.Y. Chen, Y.H. Zhang, P.C. Han. "Study on Parameters Influencing Analytical Performance of Laser-Induced Breakdown Spectroscopy". Front. Phys. 2012. 7(6): 714-720.

[10] S. Abdulmadjid, M.M. Suliyanti, K.H. Kurniawan, T.J. Lie, M. Pardede, R. Hedwig, K. Kagawa, M.O. Tjia. "An Improved Approach for Hydrogen Analysis in Metal Samples using Single Laser-Induced Gas Plasma and Target Plasma at Helium Atmospheric Pressure". Appl. Phys. B. 2006. 82: 161-166.

[11] M. Marpaung, Z.S. Lie, H. Niki, K. Kagawa, K.I. Fukumoto, M. Ramli, S.N. Abdulmadjid, N. Idris, R. Hedwig, M.O. Tjia, M. Pardede, M.M. Suliyanti, E. Jobiliong, K.H. Kurniawan. "Deuterium Analysis in Zircaloy using ps Laser-Induced Low Pressure Plasma". J. Appl. Phys. 2011. 110: 063301-1-063301-6.

[12] J. Uebbing, J. Brust, W. Sdorra, F. Leis, K. Niemax. "Reheating of a Laser-Produced Plasma by a Second Pulse Laser". Appl. Spectrosc. 1991. 45(9): 1419-1423.

[13] G. Cristoforetti, S. Legnaioli, V. Palleschi, A. Salvetti, E. Tognoni. "Characterization of a Collinear Double Pulse Laser-Induced Plasma at Several

Ambient Gas Pressures by Spectrally- and Time-Resolved Imaging". Appl. Phys. 2005. 80: 59-568.

[14] J. Scaffidi, W. Pearman, J.C. Carter, S.M. Angel. "Observations in Collinear Femtosecond–Nanosecond Dual-Pulse Laser-Induced Breakdown Spectroscopy". Appl Spectrosc. 2006. 60(1): 65-71.

[15] Y. Lu, V. Zorba, X.L. Mao, R. Zheng, R.E. Russo. "UV fs–ns Double-Pulse Laser Induced Breakdown Spectroscopy for High Spatial Resolution Chemical Analysis". J. Anal. At. Spectrom. 2013. 28: 743-748.

[16] W.L. Yip, N.H. Cheung. "Analysis of Aluminum Alloys by Resonance-Enhanced Laser-Induced Breakdown Spectroscopy: How the Beam Profile of the Ablation Laser and the Energy of the Dye Laser Affect Analytical Performance". Spectrochim. Acta Part B. 2009. 64: 315-322.

[17] C. Goueguel, S. Laville, F. Vidal, M. Sabsabi, M. Chaker. "Investigation of Resonance-Enhanced Laser-Induced Breakdown Spectroscopy for Analysis of Aluminium Alloys". J. Anal. At. Spectrom. 2010. 25: 635-644.

[18] W.D. Zhou, X.J. Su, H.G. Qian, K.X. Li, X.F. Li, Y.L. Yu, Z.J. Ren. "Discharge Character and Optical Emission in a Laser Ablation Nanosecond Discharge Enhanced Silicon Plasma". J. Anal. At. Spectrom. 2013. 28: 702-710.

[19] M. Vinić, M. Ivković. "Spatial and Temporal Characteristics of Laser Ablation Combined with Fast Pulse Discharge". IEEE Trans. Plasma Sci. 2014. 42(10): 2598-2599.

[20] K. Ali, M. Tampo, K.Akaoka, M. Miyabe, I. Wakaida. “Enhancement of LIBS Emission using Antenna-Coupled Microwave”. Opt. Express. 2013. 21(24): 29755-29768.

[21] H. Loudyi, K. Rifaï, S. Laville, F. Vidal, M. Chaker, M. Sabsabi. “Improving Laser-Induced Breakdown Spectroscopy (LIBS) Performance for Iron and Lead Determination in Aqueous Solutions with Laser-Induced Fluorescence (LIF)”. J. Anal. At. Spectrom. 2009. 24: 1421-1428.

[22] D. Giacomo, M. Dell'Aglio, O.D. Pascale, M. Capitelli. “From Single Pulse to Double Pulse ns-Laser Induced Breakdown Spectroscopy Under Water: Elemental Analysis of Aqueous Solutions and Submerged Solid Samples”. Spectrochim. Acta Part B. 2007. 62: 721-738.

[23] V.I. Babushok, F.C. DeLucia Jr., J.L. Gottfried, C.A. Munson, A.W. Miziolek. “Double Pulse Laser Ablation and Plasma: Laser Induced Breakdown Spectroscopy Signal Enhancement”. Spectrochim. Acta Part B. 2006. 61: 999-1014.

[24] M. Tampo, M. Miyabe, K. Akaoka, M. Oba, H. Ohba, Y. Maruyama, I. Wakaida. “Enhancement of Intensity in Microwave-Assisted Laser-Induced Breakdown Spectroscopy for Remote Analysis of Nuclear Fuel Recycling”. J. Anal. At. Spectrom. 2014. 29: 886-892.

[25] Y. Liu, B. Bousquet, M. Baudelet, M. Richardson. “Improvement of the Sensitivity for the Measurement of Copper Concentrations in Soil by Microwave-Assisted Laser-Induced Breakdown Spectroscopy”. Spectrochim. Acta Part B. 2012. 73: 89-92.

[26] M. Wall, Z.W. Sun, Z.T. Alwahabi. “Quantitative Detection of Metallic Traces in Water-Based Liquids by Microwave-Assisted Laser-Induced Breakdown Spectroscopy”. Opt. Express. 2016. 24(2): 1507-1517.

[27] D.K. Killinger, S.D. Allen, R.D. Waterbury, C. Stefano, E.L. Dottery. “Enhancement of Nd:YAG LIBS Emission of a Remote Target using a Simultaneous CO_2 Laser Pulse”. Opt. Express. 2007. 15(20): 12905-12915.

[28] A. Pal, R.D. Waterbury, E.L. Dottery, D.K. Killinger. “Enhanced Temperature and Emission from a Standoff 266 nm Laser Initiated LIBS Plasma using a Simultaneous 10.6 μm CO_2 Laser Pulse”. Opt. Express. 2009. 17(11): 8856-8870.

[29] M. Weidman, M. Baudelet, S. Palanco, M. Sigman, P.J. Dagdigian, M. Richardson. “Nd:YAG-CO_2 Double-Pulse Laser Induced Breakdown Spectroscopy of Organic Films”. Opt. Express. 2010. 18(1): 259-266.

[30] B. Thornton, T. Sakka, T. Masamura, A. Tamura, T. Takahashi, A. Matsumoto. “Long-Duration Nano-second Single Pulse Lasers for Observation of Spectra from Bulk Liquids at High Hydrostatic Pressures”. Spectrochim. Acta Part B. 2014. 97: 7-12.

[31] T. Sakka, H. Oguchi, S. Masai, K. Hirata, Y.H. Ogata, M. Saeki, H. Ohba. “Use of a Long-Duration ns Pulse for Efficient Emission of Spectral Lines from the Laser Ablation Plume in Water”. Appl. Phys. Lett. 2006. 88: 061120-1-061120-3.

[32] T. Sakka, A. Tamura, A. Matsumoto, K. Fukami, N. Nishi, B. Thornton. “Effects of Pulse Width on Nascent Laser-Induced Bubbles for Underwater Laser-Induced Breakdown Spectroscopy”. Spectrochim. Acta Part B. 2014. 97: 94-98.

[33] M.L. Snyder, J. Scaffidi, S.M. Angel, A.P.M. Michel, A.D. Chave. “Sequential-Pulse Laser-Induced Breakdown Spectroscopy of High-Pressure Bulk Aqueous Solutions”. Appl Spectrosc. 2007. 61(2): 171-176.

[34] J. Register, J. Scaffidi, S.M. Angel. “Direct Measurements of Sample Heating by a Laser-Induced Air Plasma in Pre-Ablation Spark Dual-Pulse Laser-Induced Breakdown Spectroscopy (LIBS)”. Appl Spectrosc. 2012. 66(8): 869-874.

[35] M. Skočić, S. Bukvić “Laser Induced Plasma Expansion and Existence of Local Thermodynamic Equilibrium”. Spectrochim. Acta Part B. 2016. 125: 103-110.

[36] O. Barthelemy, J. Margot, S. Laville, F. Vidal, M. Chaker, B. Le Drogoff, T.W. Johnston, M. Sabsabi. “Investigation of the State of Local Thermodynamic Equilibrium of a Laser-Produced Aluminum Plasma”. Appl Spectrosc. 2005. 59(4): 529-536.

[37] X.B. Zhang, Y. Deguchi, J.P. Liu. “Numerical Simulation of Laser Induced Weakly Ionized Helium Plasma Process by Lattice Boltzmann Method.” Jpn. J. Appl. Phys. 2012. 51: 01AA04.

[38] R. Payling, P. Larkins. Optical Emission Lines of the Elements. New York: John Wiley & Sons, 2000.

[39] X.L. Mao, X.Z. Zeng, S.B. Wen, R.E. Russo. “Time-Resolved Plasma Properties for Double Pulsed Laser-Induced Breakdown Spectroscopy of Silicon”. Spectrochim. Acta Part B. 2005. 60: 960-967.

[40] F. Rezaei, S.H. Tavassoli. “Quantitative Analysis of Aluminum Samples in He Ambient Gas at Different Pressures in a Thick LIBS Plasma”. Appl. Phys. B. 2015. 120: 563-571.

[41] J.M. Li, L.B. Guo, C.M. Li, N. Zhao, X.Y. Yang, Z.Q. Hao, X.Y. Li, X.Y. Zeng, Y.F. Lu. “Self-Absorption Reduction in Laser-Induced Breakdown Spectroscopy using Laser-Stimulated Absorption”. Opt. Lett. 2015. 40(22): 5224-5226.

[42] F. Paschen. “Erweiterung Der Spektren Al II, Mg I, Be I und Al I”. Ann. Phys. 1932. 404: 509-527.

[43] K.B.S. Eriksson, H.B.S. Isberg. “The Spectrum of Atomic Aluminium, Al I”. Ark. Fys. 1963. 23: 527-542.

[44] P. Risberg. “The Spectrum of Singly-Ionized Magnesium, Mg II.” Ark. Fys. 1955. 9: 483-494.

[45] G. Risberg. “The Spectrum of Atomic Magnesium, Mg I”. Ark. Fys. 1965. 28: 381-395.

[46] G. Shenstone. “The First Spectrum of Copper (Cu I)”. Philos. Trans. R. Soc. London, Ser. A. 1948. 241: 297-32

Table 1 Fe specific emission lines[38]

Element	Wavelength range (nm)	Upper level energy (cm^{-1})	A (10^8 s^{-1})
Fe-1	270-281	35611.62-38858.96	0.15-9.10
Fe-2	281-290	35379.21-36079.37	0.12-0.27
Fe-3	295-309	33095.94-34547.21	0.14-1.10
Fe-4	317-327	31307.24-32133.99	0.06-0.22
		42532.73-44411.15	0.95-4.70
Fe-5	340-350	29056.32-29732.73	0.08-0.27
Fe-6	350-368	27166.82-29056.32	0.01-0.18
		34782.41-40894.98	0.18-6.40
Fe-7	370-375	26874.55-27666.35	0.05-0.16
		33695.39-34692.14	0.22-0.90

Table 2 Comparison of SP-LIBS and DP-LIBS

Method Condition	SP-LIBS [Gate delay time: 2000-6000ns short pulse-width laser power: 18.3-35mJ/p]	DP-LIBS [Gate delay time: 2000-6000ns short pulse-width laser power: 18.3-35mJ/p inter-pulse delay time: 15-55μs]
I_{Fe-4}/I_{Fe-5} Average	0.44	0.61
I_{Fe-4}/I_{Fe-5} Standard deviation	0.071	0.038
I_{Fe-4}/I_{Fe-5} Standard deviation (%)	16%	6%
Enhancement ratio of signal intensity	- -	4.8-37.4(Fe-4) 3.0-23.0(Fe-5)

Table 3 Observed atomic and ionic spectra lines of aluminum sample[38,42-46]

Element	Wavelength (nm)	Upper level energy (cm^{-1})	A (10^8 s^{-1})
Al-1(I)	257.51	38933.97	0.28,[38] 0.36[42]
Al-2(I)	266.04	37689.41	0.26,[38] 0.28[42]
Al-3(I)	308.22	32435.45	0.63,[38] 0.59[43]
Al-4(I)	309.27	32436.80	0.74,[38] 0.73[43]
Mg-1(II)	279.55	35760.88	2.60,[38,44]
	280.27	35669.31	2.60,[38] 2.57[44]
Mg-2(I)	285.21	35051.26	4.90,[38] 4.91[45]
Cu(I)	324.75	30783.70	1.40,[38,46]
	327.40	30535.32	1.40,[38] 1.38[46]

I means atom. II means monovalent ion.

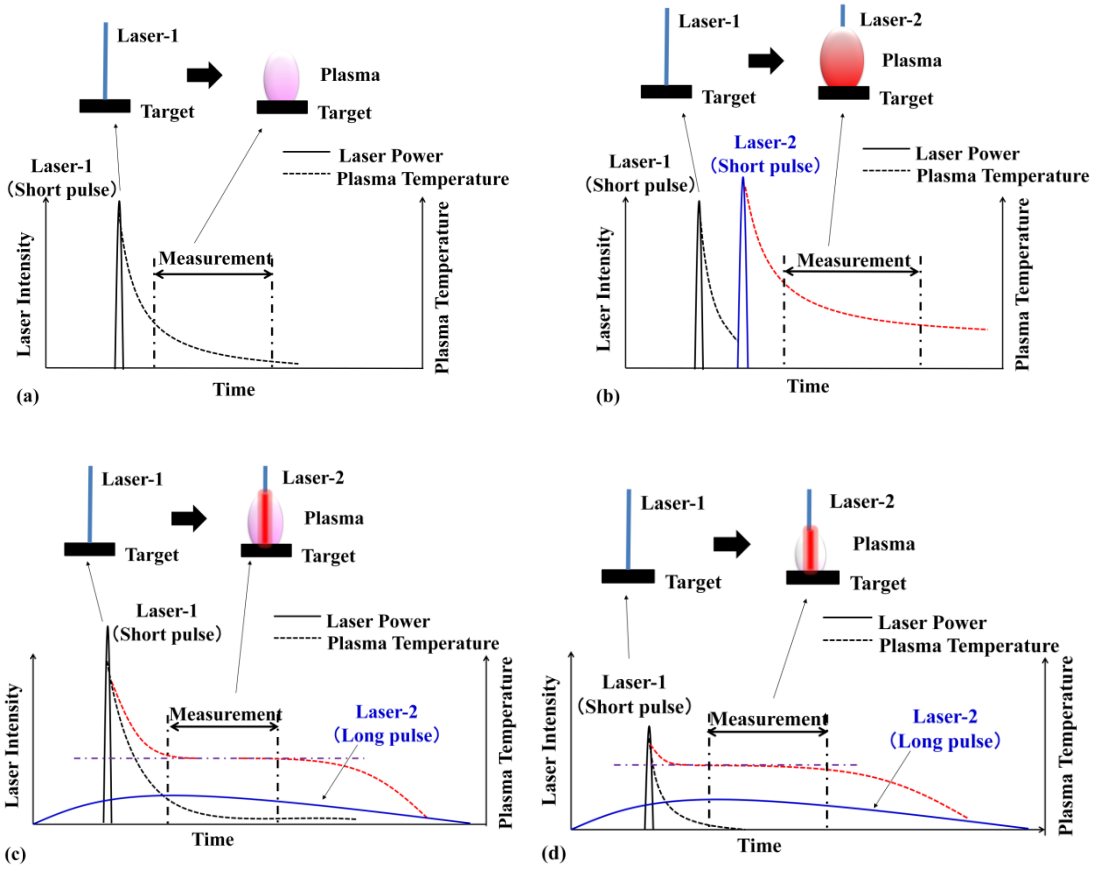

Fig. 1 Laser-induced plasma processes of single-pulse LIBS (SP-LIBS), conventional DP-LIBS and long and short DP-LIBS. (a) SP-LIBS; (b) Conventional DP-LIBS; (c) Long and short DP-LIBS with higher short pulse-width laser power; (d) Long and short DP-LIBS with lower short pulse-width laser power.

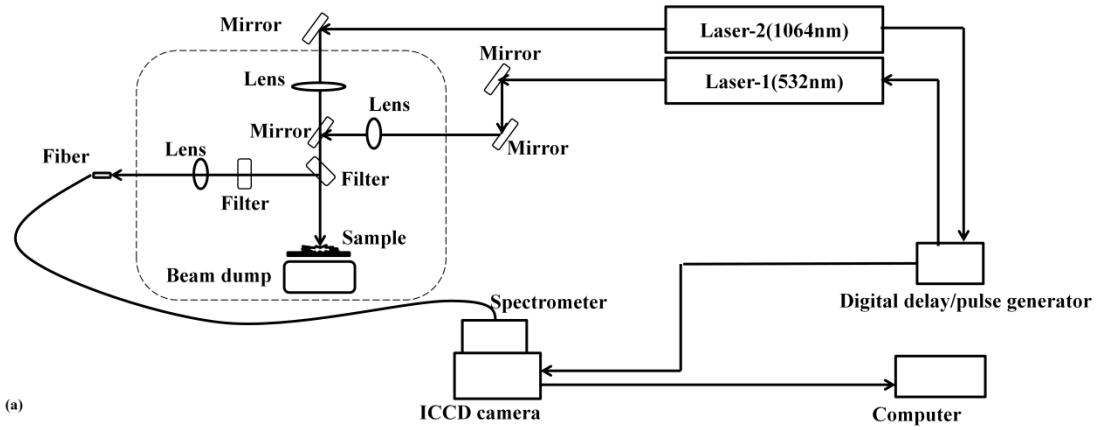

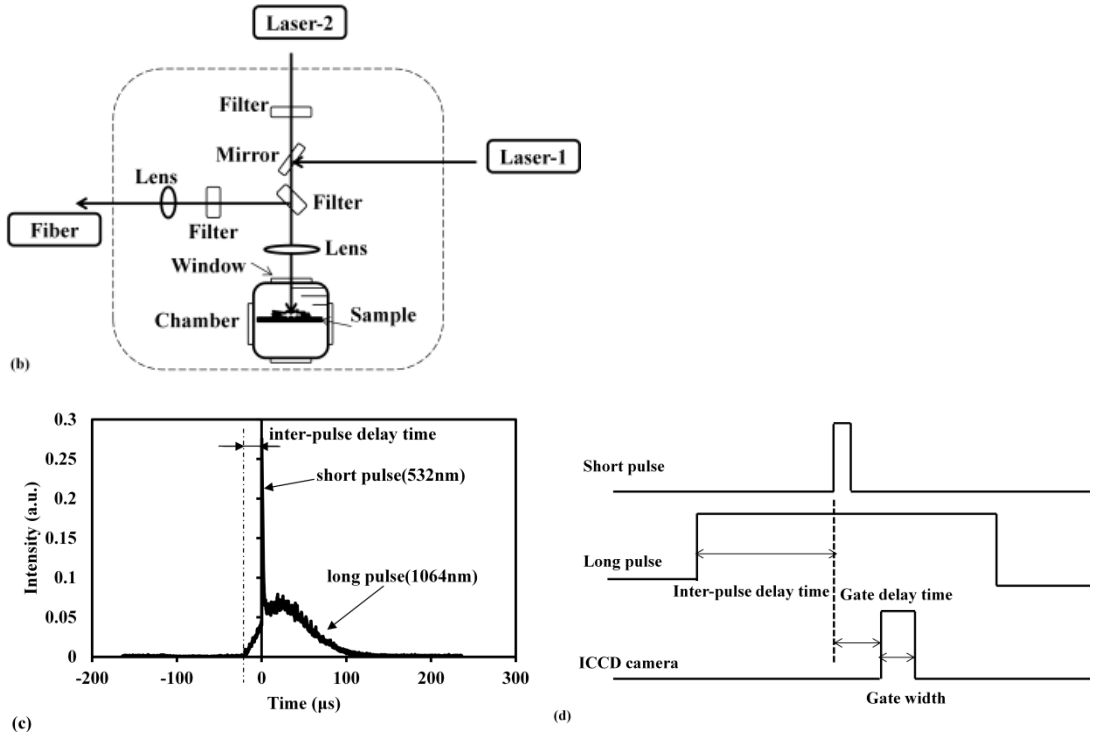

Fig. 2 Experimental setup of DP-LIBS. (a) Schematic diagram of DP-LIBS for stainless steel measurement in air; (b) Optical setup for Al sample measurement in water; (c) Pulse shapes and delay time between two pulses; (d) Different delay time.

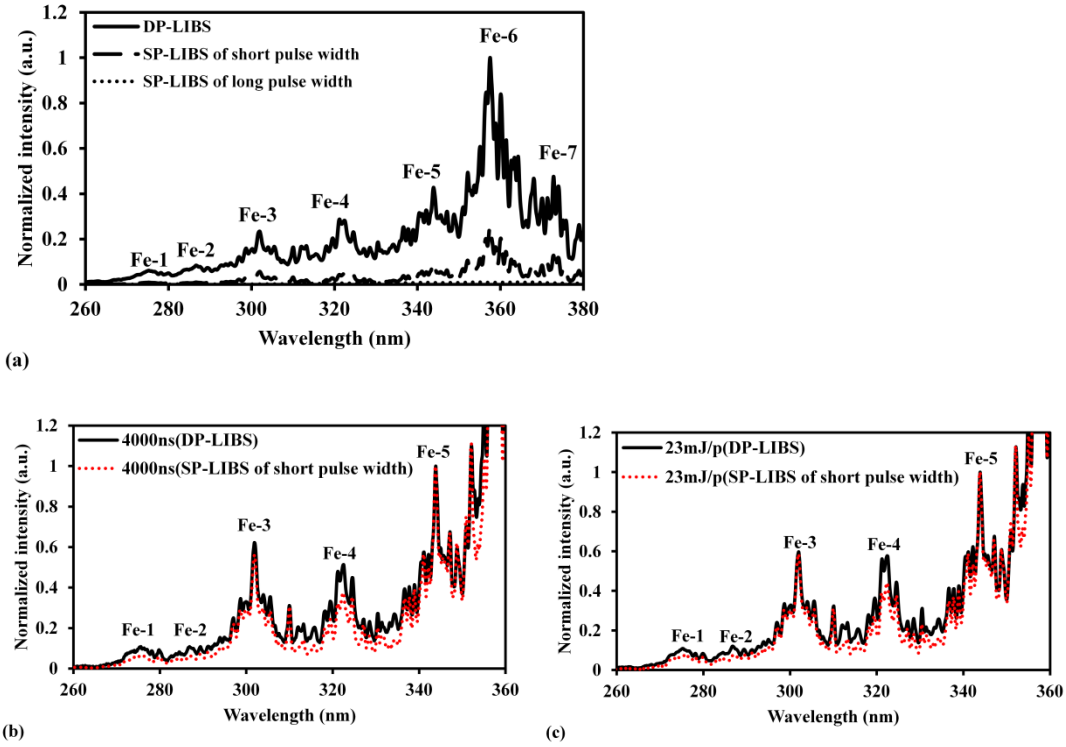

Fig. 3 Measured spectra of stainless steel in air under different conditions. (a) Comparison of SP-LIBS and DP-LIBS at short pulse-width(532 nm) laser power of 29.5 mJ/pulse and in gate delay time of 2000 ns. (b) Measured spectra using SP-LIBS of short pulse width and DP-LIBS in gate delay time of 4000 ns and at short pulse-width(532 nm) laser power of 29.5 mJ/pulse; (c) Measured spectra using SP-LIBS of short pulse width and DP-LIBS at short pulse-width laser power of 23 mJ/pulse and in gate delay time of 2000 ns. Conditions: long pulse-width(1064 nm) laser power: 400 mJ/pulse, inter-pulse delay time: 25 μs, gate width: 1000 ns.

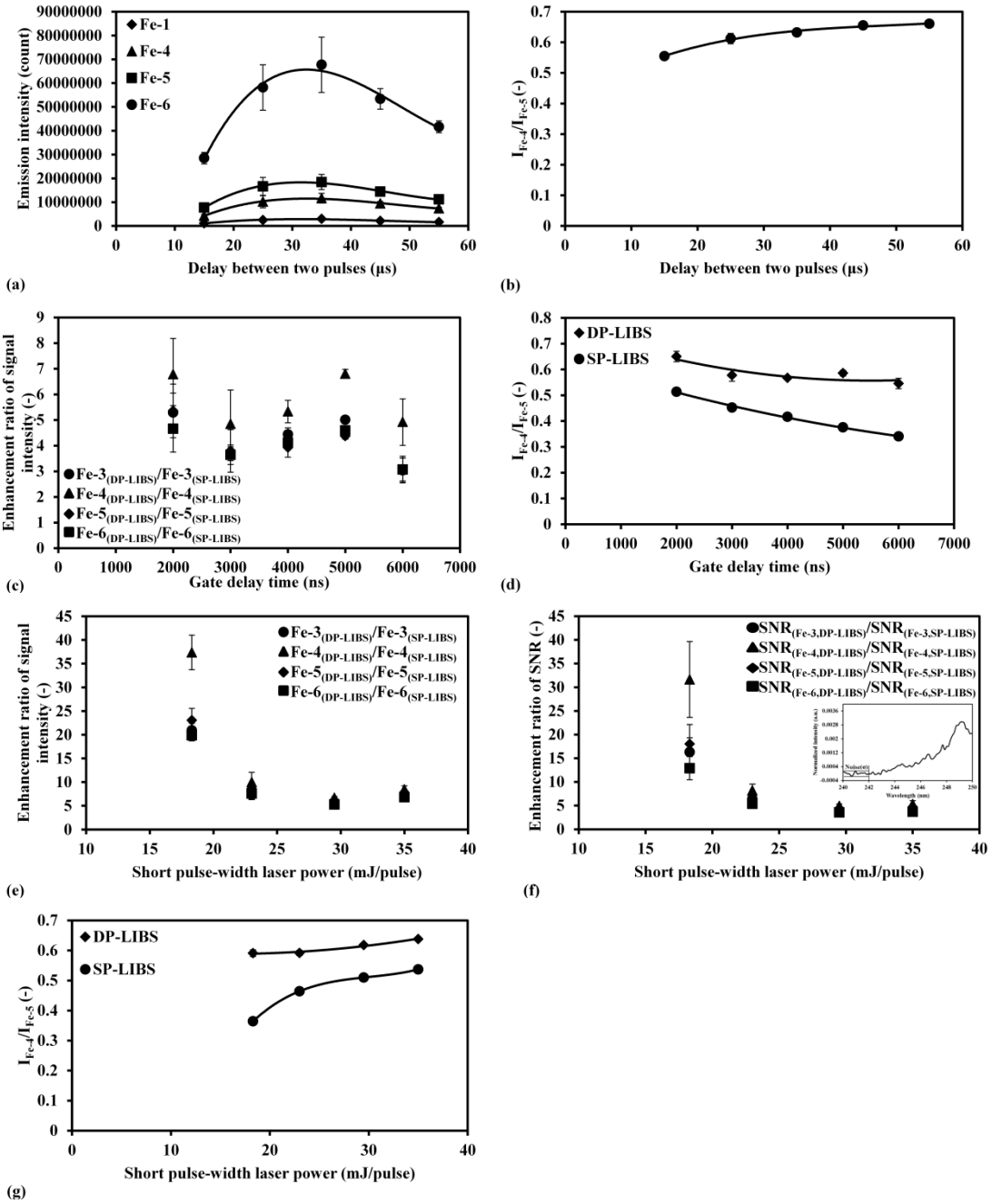

Fig. 4 Effect of different parameters on emission signals. (a) Inter-pulse delay time dependence of several Fe emission signals; (b) Inter-pulse delay time dependence of I_{Fe-4}/I_{Fe-5}. Conditions: short pulse-width(532 nm) laser power: 29.5 mJ/pulse, long pulse-width(1064 nm) laser power: 400 mJ/pulse, gate delay time: 2000 ns, gate width: 1000 ns. (c) Enhancement ratio of signal intensity using DP-LIBS and SP-LIBS of short pulse width in different gate delay time; (d) Emission intensity ratio of Fe-4 to Fe-5 in different gate delay time. Conditions: short pulse-width(532 nm) laser power: 29.5 mJ/pulse, long pulse-width(1064 nm) laser power: 400 mJ/pulse, inter-pulse delay time: 25 μs, gate width: 1000 ns. (e) Enhancement ratio at different short pulse-width laser power; (f) Enhancement ratio of signal to noise ratio(SNR); (g) Emission intensity ratio of Fe-4 to Fe-5 at different short pulse-width laser power. Conditions: long pulse-

width(1064 nm) laser power: 400 mJ/pulse, gate delay time: 2000 ns, inter-pulse delay time: 25 μs, gate width: 1000 ns.

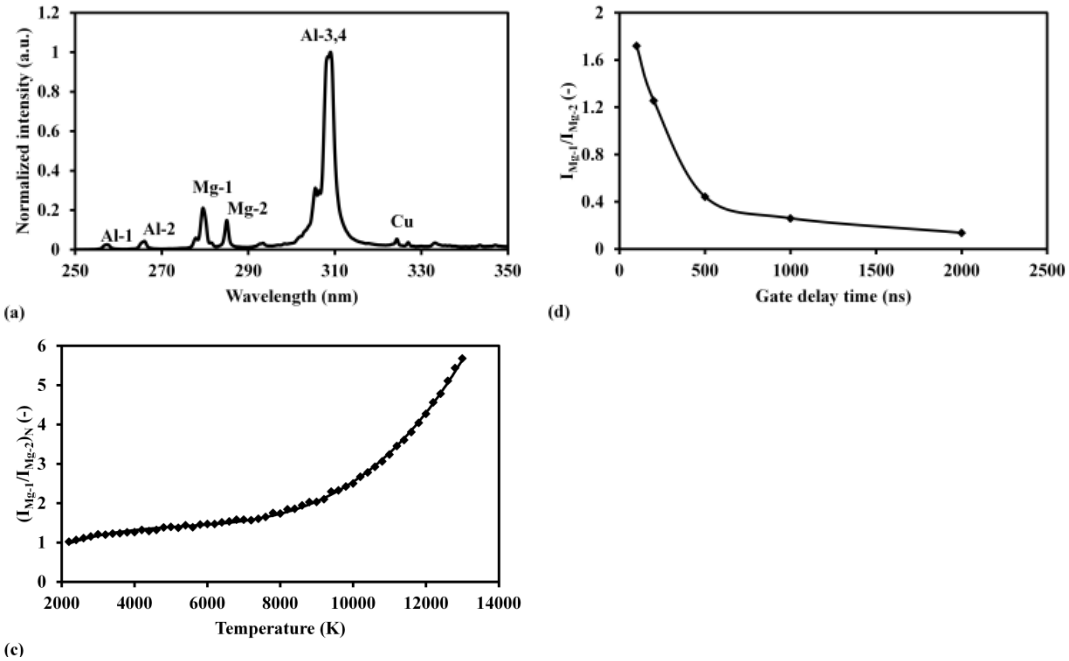

Fig.5 Measurement result of Al sample in air using SP-LIBS of short pulse width in different gate delay time. (a) Measured spectra in gate delay time of 200 ns; (b) Gate delay time dependence of I_{Mg-1}/I_{Mg-2}. Conditions: short pulse-width(532 nm) laser power: 12.2 mJ/pulse, gate width: 1000 ns. (c) The dependence of normalized I_{Mg-1}/I_{Mg-2} on plasma temperature[38]. I_{Mg-1}/I_{Mg-2} was normalized at 2000 K.

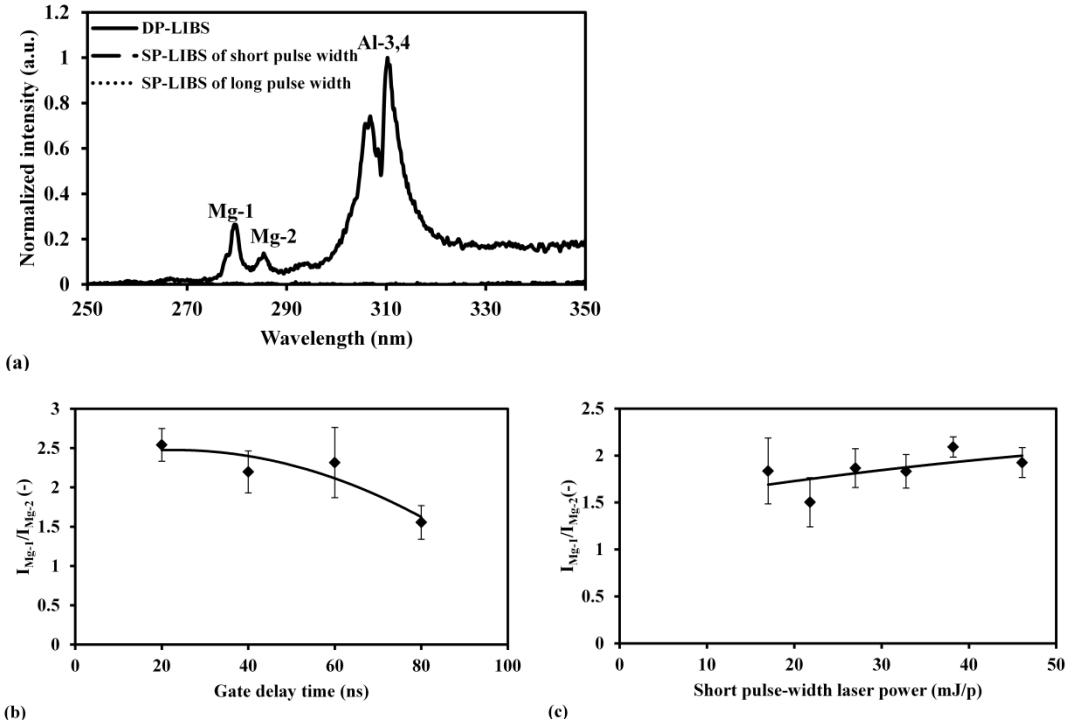

Fig. 6 Measurement results of Al sample in water under different conditions. (a) Comparison of SP-LIBS and DP-LIBS at short pulse-width(532 nm) laser power of 46.1 mJ/pulse and in gate delay time of 20 ns; (b) Gate delay time dependence of $I_{Mg\text{-}1}/I_{Mg\text{-}2}$ at short pulse-width(532 nm) laser power of 46.1 mJ/pulse; (c) Short pulse-width laser power dependence of $I_{Mg\text{-}1}/I_{Mg\text{-}2}$ in gate delay time of 40 ns. Conditions: long pulse-width(1064 nm) laser power: 500 mJ/pulse, inter-pulse delay time: 25 μs, gate width: 20 ns.